processes

MDPI

Article

Effect of Diffusion Path Lengths on Effective Moisture Diffusivity and Activation Energy of Red Delicious Apple Slices Under Convective Drying

Oldřich Dajbych, Abraham Kabutey *, Čestmír Mizera, Aleš Sedláček and David Herak

Department of Mechanical Engineering, Faculty of Engineering, Czech University of Life Sciences Prague, 165 00 Prague, Czech Republic; dajbych@tf.czu.cz (O.D.); mizera@tf.czu.cz (Č.M.); aless@tf.czu.cz (A.S.); herak@tf.czu.cz (D.H.)

* Correspondence: kabutey@tf.czu.cz; Tel.: +420-22438-3180

Abstract

The study analyzed the effect of diffusion path lengths (initial, average, and final half-thicknesses) on the shrinkage, effective moisture diffusivity, activation energy, and pre-exponential factor of thin-layer red delicious apple slices under convective drying conditions (temperature from 40 °C to 80 °C at 10 h drying time). The results show that the shrinkage increased from 31.09% at 40 °C to a maximum of 42.65% at 70 °C, then slightly decreased to 36.77% at 80 °C, indicating that shrinkage did not increase linearly with drying temperature. The diffusion path lengths yielded effective moisture diffusivities ranging from 1.43×10^{-10} to 10.31×10^{-10} m^2/s, with the average characteristic length providing the most realistic representation of the effective moisture diffusivity. The high coefficient of determination ($R^2 = 0.965$), consistent with the model efficiency value, confirms that the Arrhenius model fits the experimental diffusivity data across the temperature range studied. The mean absolute percentage error of 12% between the experimental and predicted diffusivities confirms the reliability of Fick's and Arrhenius models. The activation energy ranged from 21.56 to 26.03 kJ/mol across diffusion path lengths, indicating a moderate sensitivity of moisture diffusion to temperature.

Keywords: drying kinetics; Fick's second law; Arrhenius model; moisture transport; diffusion behaviour

1. Introduction

Apples are among the fruits and vegetables that have a high moisture content, ranging from 80% to 95% on a wet basis [1,2]. They are classified as highly perishable commodities and are susceptible to microbial infection and spoilage during storage [3,4]. Drying can reduce the moisture content and extend the shelf life of fruits and vegetables [5,6]. Convective (hot-air oven) drying, microwave drying, infrared drying, and freeze drying are among the drying techniques; however, hot-air oven drying is the most widely used method [7,8]. Food drying is a complex process involving heat and moisture transfer [9–13]. Knowledge of the moisture transport process is essential for understanding and accurately modelling the food drying process [14,15]. Effective moisture diffusivity is a critical parameter for characterizing intrinsic moisture transfer mechanisms during the drying process [11,16]. It describes the movement of moisture within the product and is a key transport property in the mathematical modelling of various food processes, including drying [16–18]. Fick's mathematical model explicitly relates moisture diffusivity with drying rates, especially

Check for updates

Academic Editor: Blaž Likozar

Received: 17 May 2026
Revised: 13 June 2026
Accepted: 18 June 2026
Published: 21 June 2026

Copyright: © 2026 by the authors. Licensee MDPI, Basel, Switzerland. This article is an open access article distributed under the terms and conditions of the Creative Commons Attribution (CC BY) license.

during the falling-rate drying stage [19,20]. Several studies have successfully applied Fick's model to determine the average effective moisture diffusivity of different food materials using the slope method, assuming constant moisture diffusivity throughout the drying process [21,22]. The influence of drying temperature on moisture diffusivity is commonly described using an Arrhenius-type relationship [21,23]. Studies have shown that both moisture and temperature significantly affect moisture diffusivity in biological and food materials [9,17]. Recently, drying various fruit slices such as peach, apricot, apple, orange, kiwi, and banana has become common, and the dried products are sold at relatively high prices in the market [24]. In the literature, several drying techniques and pretreatments have been applied to different varieties of apple slices, with the aim of evaluating the drying kinetics, colour change, quality attributes, microstructure, moisture diffusivity, activation energy, and energy and exergy analyses [25–31]. The development of energy-efficient, cost-effective, and high-quality drying techniques has been a current research trend [9,26].

In our previously published study on red delicious apple slices [27], the effective moisture diffusivity and activation energy were not described based on the study objectives, which mainly focused on colour parameters, rehydration rate, shrinkage and thin-layer mathematical models for fitting the drying curves. However, the physical and thermal properties of agricultural products, such as mass and heat transfer, moisture distribution, and activation energy, are essential for designing optimal drying equipment [24,32]. Activation energy is obtained by plotting the natural logarithm of the effective moisture diffusivity against the reciprocal of the absolute temperature. By applying Fick's second law and treating the sample slices as infinite-thin slabs, the effective moisture diffusivity can be calculated [24]. According to Barforoosh et al. [24], the assumptions for isothermal conditions in both activation energy and effective moisture diffusivity calculations include uniform initial moisture distribution throughout the sample, uniform mass transfer toward the centre, equilibrium between surface moisture content and ambient air, negligible external resistance compared to internal resistance and moisture movement occurring solely by diffusion. These assumptions are consistent with those applied in the previously published study.

Most importantly, the effect of the dry basis moisture content based on the final weight of the sample after drying and the diffusion path lengths on the effective moisture diffusivity and activation energy of thin-layer apple slices by using Fick's and Arrhenius models has not been distinctly reported in the literature among varying drying techniques [25,26]. The relationship between dry basis moisture content and drying time provides a direct representation of the reduction in water content during drying. The drying curve pattern (sample weight, moisture content and moisture ratio in relation to drying time) indicates the rate of moisture removal and reflects the influence of drying temperature on the drying process. Generally, higher drying temperatures enhance heat and mass transfer, thereby accelerating moisture evaporation from the material surface and internal structure [30,32].

This present study adopted the simplified drying approach, where the final mass obtained after drying at each temperature was assumed to represent the true dry mass of the apple slices for determining the dry basis moisture content and moisture ratio. Therefore, the objectives of the study were to determine the effective moisture diffusivity, activation energy and pre-exponential factor of dried red delicious apple slices under convective drying for varying diffusion path lengths and to compare the range of values reported in the literature based on the reference method, where the true dry mass was utilized in the determination of the dry basis moisture content.

2. Materials and Methods

2.1. Sample and Hot-Air Oven Drying Method

Fresh whole red delicious apples (Figure 1a) were purchased from a supermarket in Prague, Czech Republic. The samples were stored in a refrigerator at 5 °C. Before the experiments, the samples were removed and allowed to equilibrate to laboratory conditions of 24.26 ± 0.50 °C and 41.6 ± 2.42% relative humidity. A slicer (SFS 4050SS, Prague, Czech Republic) was used to cut the whole fresh apples into two cylindrical slices with a thickness of 8.07 ± 0.05 mm and a diameter of 66.27 ± 3.13 mm (Figure 1b). In total, ten whole apple samples were used across the drying temperatures. The dimensions (diameter and thickness) of both fresh and dried apple slices were measured using a digital calliper with an accuracy of 0.01 mm. The weights of the samples were measured using a digital balance (KERN & SOHN 440–35, Balingen, Germany) with an accuracy of 0.01 g. A standard hot-air oven (MEMMERT UF55m GmbH + Co. KG, Buechenbach, Germany) was used to dry the thin-layer apple slices (Figure 1c) at temperatures ranging from 40 °C to 80 °C, with a 10 °C interval, for 10 h. Air circulation in the oven during drying was controlled by setting both the fan and the restrictor air flap to 30%. The oven allows adjustment in 10% increment up to 100%. The 30% setting may be approximated to an air velocity range of 0.2–0.8 m/s, based on the internal chamber dimensions of 400 × 400 × 300 mm, corresponding to a volume of 0.053 m^3. A load cell (0–100 g) connected to an HX711 AD converter (AVIA, Shenzhen, China) with software temperature compensation was used for the weight data recording. A digital sensor DS18B20 (Maxim Integrated Products GmbH, Landsberger, Munich, Germany) was used to monitor the temperature inside the oven. Sample weight, in relation to the drying time and temperature, was recorded every 60 s. The drying process was automated, and the recorded data was transported to Microsoft Excel for cleaning and subsequent calculations.

Figure 1. (**a**) Two fresh samples of whole red delicious apples, (**b**) fresh thin-layer slice sample and (**c**) dried sample at 80 °C as a representative of samples dried at 40, 50, 60 and 70 °C.

2.2. Dry Basis Moisture Content

The dry basis moisture content of the samples in fraction was calculated using (Equation (1)) [33–35].

$$M_t = \frac{W_t - W_d}{W_d} \quad (1)$$

where M_t is the dry basis moisture content of the sample (g/g) at the moment of drying time t (s), W_t is the initial mass of the sample (g) and W_d is the final weight of the sample (g) at 10 h drying across the drying temperatures between 40 °C and 80 °C.

2.3. Moisture Ratio

The moisture ratio was calculated using (Equation (2)) [36–38].

$$MR = \frac{M_t - M_e}{M_0 - M_e} \tag{2}$$

where MR is the moisture ratio (dimensionless), M_0 is the initial dry-basis moisture content (g/g), and M_e is the equilibrium moisture content (dry basis, often minimal and assumed negligible for many cases). The value of M_e can be neglected, as it is relatively small compared to the values of M_t and M_0. Therefore, (Equation (2)) can be rewritten in the form given in (Equation (3)) [37,39].

$$MR = \frac{M_t}{M_0} \tag{3}$$

2.4. Shrinkage

The shrinkage was calculated as the percentage reduction in characteristic length of the sample from the initial state to the final state (Equation (4)), ensuring positive values for all drying conditions [40,41].

$$SK = \left(\frac{L_i - L_f}{L_i}\right) \times 100 = \left(1 - \frac{L_f}{L_i}\right) \times 100 \tag{4}$$

where SK is the shrinkage (%), L_i is the initial thickness and L_f is the final thickness, which represents the characteristic length of the sample based on Fick's second law.

2.5. Effective Moisture Diffusivity

In many drying processes, especially thin-layer drying, the moisture ratio (MR) follows Fick's second law (Equation (5)) [38,42].

$$MR = \frac{8}{\pi^2}\exp\left(-\frac{\pi^2 D_{eff} t}{4L^2}\right) \tag{5}$$

Taking logs of (Equation (5)) gives (Equation (6)) as follows:

$$\ln(MR) = ln\left(\frac{8}{\pi^2}\right) - \frac{\pi^2 D_{eff}}{4L^2} t \tag{6}$$

Plotting $ln(MR)$ versus time, the slope gives (Equation (7)) as follows:

$$D_{eff} = -\frac{4L^2 \times slope}{\pi^2} \tag{7}$$

where D_{eff} is the effective moisture diffusivity (m^2/s) and L is the half-thickness (m) characteristic length of the apple slice. The slope was determined from the plot of $\ln(MR)$ versus drying time, where a fixed threshold of $MR \leq 0.3$ was maintained across drying temperatures. This threshold was chosen because several drying studies assume that the falling-rate diffusion-controlled period is dominant at low values and that Fick's law approximation is valid in this region [21,24].

2.6. Activation Energy

Based on the diffusivity data at different drying temperatures, the Arrhenius equation can be fitted following (Equations (8)–(10)) [38,42].

$$D_{eff} = D_0 \exp\left(-\frac{E_a}{RT}\right) \quad (8)$$

where D_0 is the pre-exponential factor (m^2/s). Taking logs of (Equation (8)) gives (Equation (9)) as follows:

$$ln\left(D_{eff}\right) = ln(D_0) - \frac{E_a}{R}\left(\frac{1}{T}\right) \quad (9)$$

From a plot of $ln(D_{eff})$ versus 1/T, the slope gives (Equation (10)) as follows:

$$E_a = -(slope) \times R \quad (10)$$

where E_a is the activation energy (kJ/mol), T is the absolute temperature (K) and R is the universal gas constant with the value of 8.314 J/mol·K.

2.7. Statistics Analysis

The experiments were conducted in duplicate, and the data were presented as means, standard deviation, and percentage coefficient of variation. Comparison of models was evaluated based on the coefficient of determination, root mean square error, mean absolute error, mean absolute percentage error and model efficiency. Graphical illustrations were generated using Statistica 13 software [43]. All calculations, descriptive statistics and model fitting metrics were performed using Microsoft Excel (version 2601).

3. Results and Discussion

3.1. Half-Thickness Characteristic Length

In Fick's second law for slab-shaped materials such as thin-layer apple slices, the effective moisture diffusivity (Equation (7)) is related to the slope of the natural logarithm of the moisture ratio versus drying time [38,42]. The half-thickness characteristic length (L) of the sample directly affects the effective moisture diffusivity quadratically. The initial half-thickness, the final half-thickness and the average half-thickness of the fresh and dried apple slices were considered for the estimation of the effective moisture diffusivity, activation energy and pre-exponential factor. The initial thickness represents the initial diffusion path for moisture before shrinkage starts. The final thickness represents the shortest diffusion path after maximum shrinkage. The average thickness represents an effective or average diffusion distance across the entire drying period. Kidane et al. [9] used the average thickness of 0.00525 m of apple slices, yielding a half-thickness of 0.002625 m, in computing the effective moisture diffusivity. In this study, the half-thickness characteristic lengths (Table 1) were used to compute the parameters of the Fick's second law and Arrhenius model, which are discussed in the succeeding sections.

Table 1. Half-thickness characteristic lengths of dried apple slices during convective drying temperatures.

T_{PR} (°C)	Test I			Test II		
	L_i (m)	L_f (m)	L_{avg} (m)	L_i (m)	L_f (m)	L_{avg} (m)
40	0.00375	0.00273	0.00324	0.00385	0.00250	0.00317
50	0.00375	0.00220	0.00297	0.00393	0.00247	0.00320

Table 1. *Cont.*

T_{PR} (°C)	Test I			Test II		
	L_i (m)	L_f (m)	L_{avg} (m)	L_i (m)	L_f (m)	L_{avg} (m)
60	0.00415	0.00228	0.00322	0.00402	0.00247	0.00325
70	0.00407	0.00242	0.00324	0.00412	0.00228	0.00320
80	0.00410	0.00276	0.00343	0.00417	0.00247	0.00332

T_{PR}: Drying temperature; L_i: initial half-thickness; L_f: final half-thickness; and L_{avg}: average half-thickness.

3.2. Drying Behaviour: Weight, Moisture Content and Moisture Ratio

The drying behaviour of thin-layer red delicious apple slices was evaluated through changes in sample weight, moisture content, and moisture ratio over drying time at temperatures ranging from 40 to 80 °C (Figure 2a–f). A consistent decreasing trend was observed across all parameters, with higher drying temperatures producing steeper curves and shorter drying durations. At the initial stage, rapid reductions in weight and moisture content occurred due to the removal of free and surface moisture, followed by a gradual decline as the process transitioned into the falling-rate period, where internal diffusion became the dominant mechanism. This behaviour reflects the increasing resistance to moisture migration within the sample matrix as drying progresses [3,22]. The moisture content and moisture ratio exhibited typical exponential decay patterns with drying time, confirming that moisture transport is governed primarily by diffusion processes [44,45]. Elevated temperatures enhanced the vapour pressure gradient and increased effective moisture diffusivity, thereby accelerating water removal and reducing the time required to reach equilibrium conditions. In contrast, lower temperatures resulted in slower moisture migration and extended drying periods due to reduced thermal energy and diffusivity. These findings are consistent with diffusion-based drying models and temperature-dependent behaviour of agricultural products [44–48].

However, it is important to highlight that the dry basis moisture content calculation produces noticeably higher moisture content values at higher drying temperatures (Figure 2c,d). This behaviour could result from the use of the final drying mass at each temperature as the true dry mass in the moisture content equation (Equation (1)). Since higher temperatures produced lower final masses, the denominator of the dry-basis equation became smaller, thereby mathematically amplifying the calculated moisture content values. The elevated moisture content curves observed at higher temperatures reflect not only enhanced drying behaviour but also the scaling effect associated with the simplified calculation approach. Therefore, the resulting moisture content curves should be interpreted as apparent drying characteristics suitable primarily for engineering and comparative drying analyses. On the contrary, the moisture ratio curves (Figure 2e,f) do not represent the absolute moisture amount. Instead, it represents the fraction of moisture removal remaining in the sample relative to the initial condition. Thus, all drying curves are rescaled to begin at the same point regardless of sample mass, dry-mass definition and drying temperature. In fact, the moisture ratio is a normalized parameter, and the normalization process minimizes scaling differences between the simplified and the reference approaches, even though the effective moisture diffusivity, activation energy and the Arrhenius diffusion (pre-exponential) factor may still differ because they depend on the logarithmic moisture ratio slope [38,42].

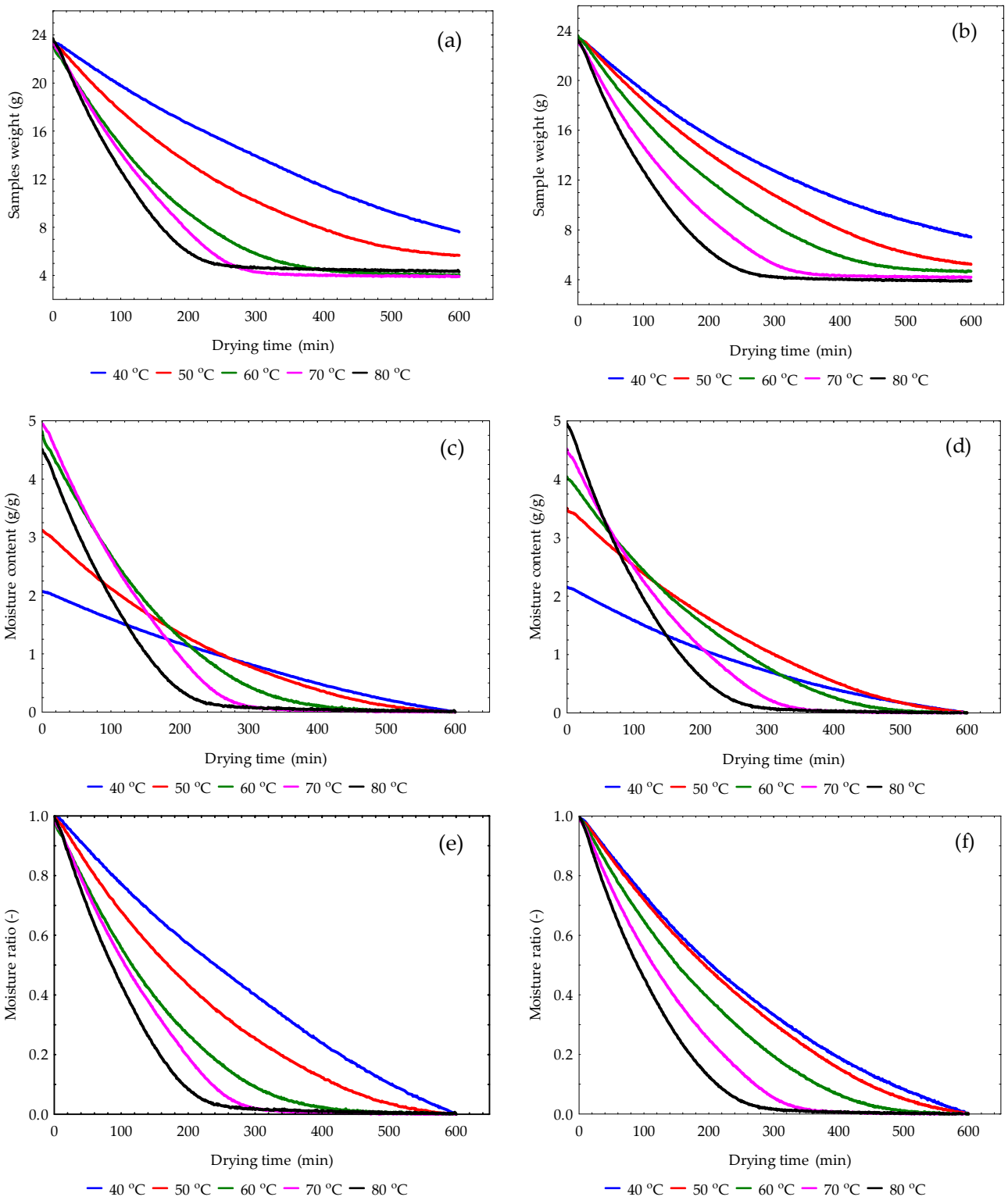

Figure 2. Drying curves of thin-layer red delicious apple slices across drying temperature for 600 min: (**a**,**b**) sample weight, (**c**,**d**) moisture content and (**e**,**f**) moisture ratio for duplicated tests I and II.

3.3. Linear Fits and Effective Moisture Diffusivity Across Characteristic Lengths

The calculation of the effective moisture diffusivity D_{eff} using equation (7) requires both the half-thickness of the sample and the slope obtained from the linear relationship between the natural logarithm of the moisture ratio and drying time for the duplicated experiments, graphically displayed in Figure 3a,b. The determined slope values, coefficients of determination (R^2), and corresponding D_{eff} values for the varying characteristic lengths

are presented in Table 2. The linear regression models exhibited a strong fit, with R^2 values ranging from 0.996 to 0.997, confirming the reliability of Fick's second law for describing the falling-rate period in apple slice drying. During this stage, the material surface is no longer saturated, and the drying rate is governed by internal moisture diffusion from the solid interior to the surface [46,49]. Higher temperatures enhance surface evaporation and promote internal moisture movement as water molecules require less activation energy for diffusion due to increased vapour pressure, reduced viscosity, and greater mobility of bound water. Additionally, temperature-induced physical and microstructural changes, such as cell wall rupture and shrinkage, further facilitate moisture transport. As a result, higher D_{eff} values correspond to faster internal moisture migration leading to shorter drying times, whereas lower temperatures lead to reduced diffusivity and prolonged drying durations [9,45].

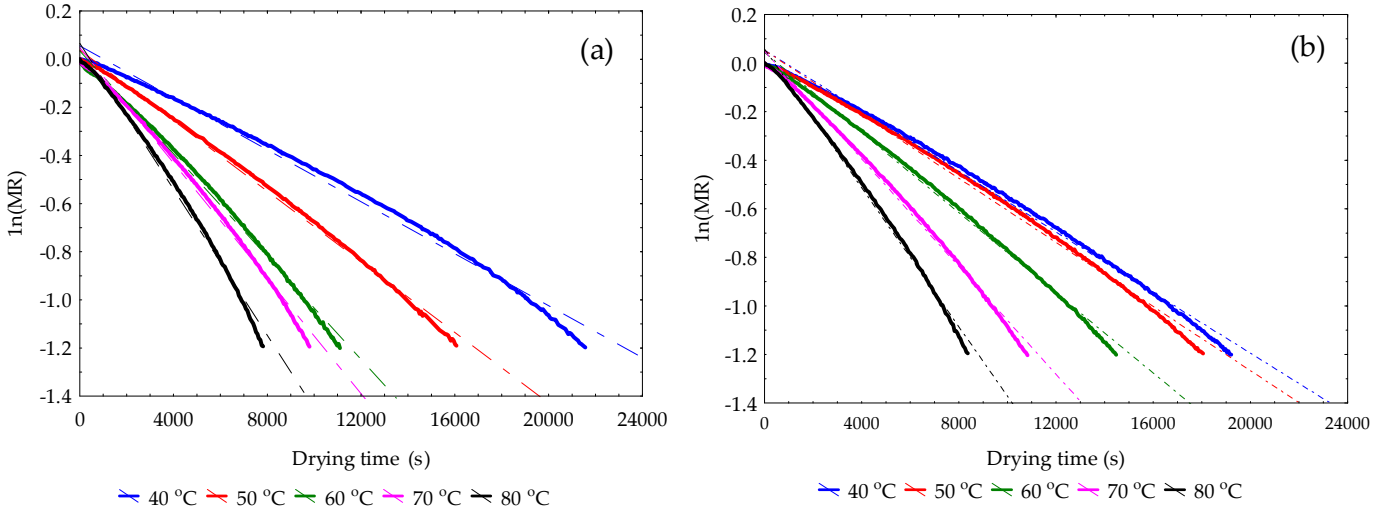

Figure 3. Linear fits of thin-layer samples under hot-air oven drying for (**a**) test I and (**b**) test II.

Table 2. Determined effective moisture diffusivity across diffusion path lengths and drying temperature for duplicated tests.

Tests	T_{PR} (°C)	Slope $\times 10^{-5}$	R^2	Initial Length, D_{eff} (m^2/s) $\times 10^{-10}$	Final Length, D_{eff} (m^2/s) $\times 10^{-10}$	Average Length D_{eff} (m^2/s) $\times 10^{-10}$
I	40	−5.399	0.993	3.077	1.631	2.297
I	50	−7.337	0.997	4.170	1.433	2.623
I	60	−10.685	0.996	7.458	2.251	4.476
I	70	−11.985	0.995	8.026	2.833	5.099
I	80	−15.169	0.993	10.309	4.666	7.212
II	40	−6.239	0.996	3.737	1.581	2.545
II	50	−6.590	0.996	4.125	1.623	2.731
II	60	−8.254	0.997	5.406	2.041	3.523
II	70	−11.081	0.996	7.605	2.324	4.585
II	80	−14.295	0.996	10.050	3.520	6.367

T_{PR}: Temperature; D_{eff}: Effective moisture diffusivity and R^2: Coefficient of determination.

For the duplicated experiments, D_{eff} values calculated using the initial half-thickness were consistently the highest, followed by those based on the average half-thickness, while the final half-thickness yielded the lowest values. This pattern reflects the quadratic dependence of diffusivity on characteristic length and the progressive shrinkage of the sample during drying. Using the initial thickness tends to overestimate D_{eff}, as it assumes a constant

diffusion path despite shrinkage. The effective diffusion path shortens as the sample loses moisture and collapses structurally. In contrast, the final thickness underestimates D_{eff} because it represents only the end-stage geometry when diffusion is minimal. The average half-thickness therefore provides a more realistic estimate, representing the mean diffusion distance throughout the drying process. Consequently, the average characteristic length is preferred for diffusivity analysis in materials undergoing continuous shrinkage [47,48]. The calculated D_{eff} values ranged from 1.43×10^{-10} to 10.31×10^{-10} m^2/s, which increased with drying temperature. Kidane et al. [9] reported values between 1.990×10^{-7} and 2.0599×10^{-7} m^2/s for apple slices dried under solar dryers using average thickness. Yilmaz et al. [44] observed values ranging from 6.81×10^{-10} to 3.27×10^{-8} m^2/s for dried apricot under different pretreatments. Arulkumar et al. [45] reported D_{eff} values for paneer samples ranging from 2.15×10^{-8} to 2.40×10^{-8} m^2/s at 50 °C, 2.19×10^{-8} to 2.68×10^{-8} m^2/s at 55 °C, and 3.61×10^{-8} to 3.85×10^{-8} m^2/s at 60 °C. The values obtained in this study fall within typical D_{eff} range of 10^{-8} to 10^{-12} m^2/s reported for food products [50–52].

3.4. Shrinkage Behaviour of Apple Slices

Shrinkage, defined as the reduction in volume and shape, cannot be neglected in drying processes [41,53]. The shrinkage values of apple slices at drying temperatures ranging from 40 to 80 °C are presented in Table 3. Both tests showed a decrease in slice thickness during drying, confirming that shrinkage results from moisture removal and structural collapse of the cellular matrix [54,55]. In test I, shrinkage increased from 27.2% at 40 °C to a maximum of 45.1% at 60 °C, then gradually declined to 32.7% at 80 °C. Similarly, in test II, shrinkage rose from 34.98% at 40 °C to 44.71% at 70 °C, before slightly decreasing to 40.82% at 80 °C. The mean shrinkage followed a similar trend, increasing from 31.09% at 40 °C to a peak of 42.65% at 70 °C, then decreasing to 36.77% at 80 °C. The lowest standard deviation (2.91) was observed at 50 °C and 70 °C, indicating high repeatability and stable shrinkage behaviour. In contrast, the higher standard deviation values (4.59–5.70) at 40 °C and 80 °C suggest greater variability, likely due to uneven moisture gradients. The percentage coefficient of variation remained below 18%, indicating good reproducibility of the results. These results indicate that shrinkage does not increase linearly with temperature but instead reaches a peak within the mid-temperature range (60–70 °C), followed by a slight reduction. This behaviour suggests that moderate temperatures promote uniform moisture loss and structural softening, whereas higher temperatures may induce surface hardening, limiting further structural collapse [53,55]. Differences in peak shrinkage between tests I and II may be attributed to minor variations in sample uniformity or airflow conditions during the tests. Similar trends have been reported in the literature. Mayor and Sereno [15] and Hatamipour and Mowla [55] noted that fruit tissues often exhibit maximum shrinkage at moderate temperatures due to a balance between internal vapour pressure and cell wall plasticity. In general, shrinkage is rarely negligible in food systems and should be considered when predicting moisture content distribution during drying. Moisture loss and heating generate internal stresses within the cellular structure, leading to deformation and dimensional reduction [15]. The relationship between shrinkage and the drying temperature is shown in Figure 4. A polynomial model provided a better fit ($R^2 = 0.985$) than a linear model ($R^2 = 0.249$), confirming the non-linear nature of shrinkage behaviour with temperature.

Table 3. Shrinkage for apple slices under hot-air oven drying and their statistical metrics.

T_{PR} (°C)	Test I Shrinkage (%)	Test II Shrinkage (%)	Mean	SD	% CV
40	27.200	34.980	31.090	5.502	17.696
50	41.389	37.277	39.333	2.907	7.391
60	45.060	38.557	41.809	4.598	10.999
70	40.590	44.714	42.652	2.916	6.837
80	32.723	40.816	36.770	5.723	15.564

T_{PR}: Temperature; SD: Standard deviation; CV: Coefficient of variation.

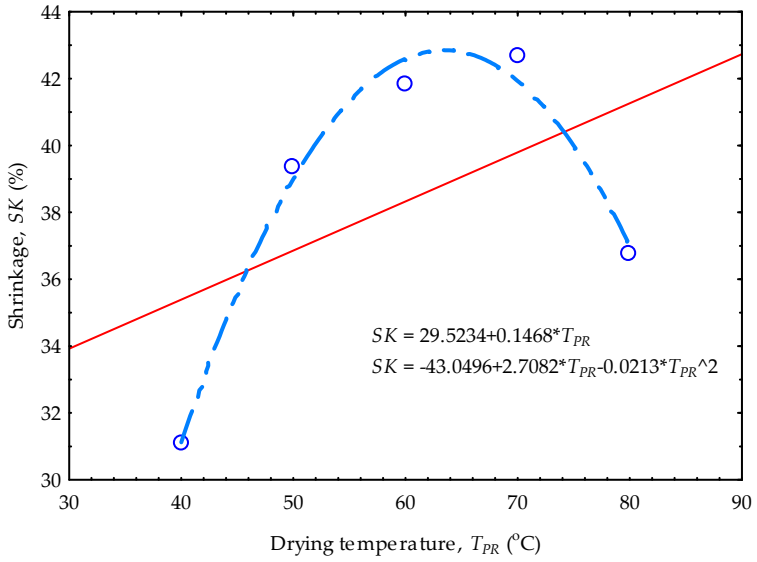

Figure 4. Relationship between shrinkage and drying temperature of dried apple slices. The blue dashed line represents the polynomial fit, and the red line indicates the linear fit. *: multiplication sign and the superscript ^2 indicate quadratic term.

3.5. Relationship Between Shrinkage and Effective Moisture Diffusivity

Shrinkage directly influences the effective moisture diffusivity D_{eff} by reducing the diffusion path length and altering the internal pore structure [53,54]. The observed 27–45% reduction in sample thickness indicates a corresponding decrease in diffusion distance, which may lead to an overestimation of D_{eff} if geometric changes are not considered. Therefore, accounting for shrinkage using average half-thickness provides a more realistic representation of time-averaged internal moisture transport. The results from both experimental tests confirm that neglecting shrinkage can lead to overestimation of D_{eff} values, particularly within the mid-temperature range where structural collapse is most pronounced. Temperature was also found to strongly influence the magnitude and progression of shrinkage. Maximum deformation occurred between 60 and 70 °C, while a slight reduction at 80 °C can be attributed to case hardening and reduced surface flexibility [54,55].

3.6. Activation Energy Across Characteristic Lengths

The activation energy E_a represents the minimum energy required to initiate moisture diffusion and overcome resistance during the drying process [33,44]. The Arrhenius plots of the natural logarithm of effective moisture diffusivity, D_{eff} versus the reciprocal of absolute temperature, $1/T_{PR}$ (K^{-1}) for both test conditions, and the three characteristic lengths are shown in Figure 5, with the corresponding E_a values presented in Table 4. The coefficients of determination (R^2) ranged from 0.8547 to 0.9622 across all conditions. At higher values (≈0.96), the Arrhenius model shows a strong fit, indicating that temperature has a dominant and predictable influence on D_{eff}. The linear behaviour confirms that moisture diffusion is

primarily thermally activated [44,45]. At lower R^2 values (≈0.85), the relationship remains strong but with greater scatter, suggesting that additional factors such as sample variability or moisture-dependent diffusivity may also influence the results [41]. The calculated E_a values ranged from 17.829 to 28.399 kJ/mol, depending on the characteristic length and test condition. These values fall within the typical range (6.80–78.93 kJ/mol) reported for food materials [56–59].

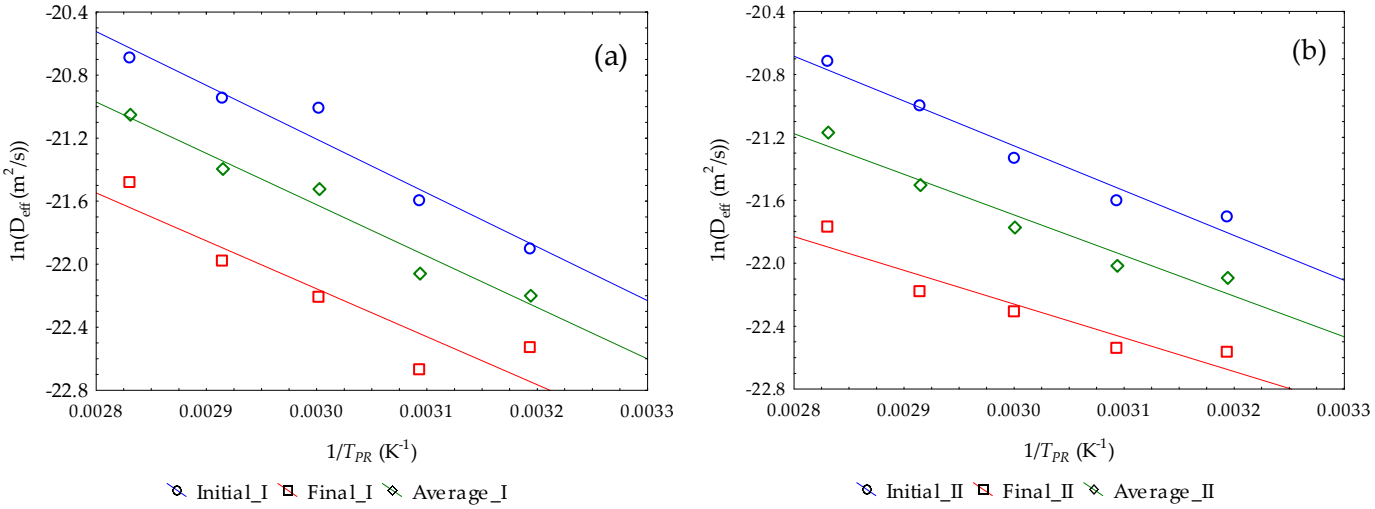

Figure 5. Arrhenius plots of the natural logarithm of the effective moisture diffusivity (D_{eff}) and inverse absolute temperature (T_{PR}) for half-thickness characteristic lengths for duplicated tests (**a**) test I and (**b**) test II.

Table 4. Descriptive statistics for evaluating the activation energy (E_a) across characteristic lengths of dried apple slices.

Characteristic Length, *L* (m)	Test I E_a (kJ/mol)	Test II E_a (kJ/mol)	Mean	SD	% CV
Initial length	28.399	23.669	26.034	3.344	12.845
R^2	0.951	0.962	0.957	0.007	0.762
Final length	25.289	17.829	21.559	5.276	24.470
R^2	0.855	0.886	0.870	0.022	2.503
Average length	27.119	21.462	24.291	4.001	16.470
R^2	0.962	0.948	0.955	0.010	1.066

R^2: Coefficient of determination; SD: Standard deviation, and CV: Coefficient of variation.

E_a showed a clear dependence on the characteristic length used in the analysis. For test I, E_a decreased from 28.40 kJ/mol (initial half-thickness) to 25.29 kJ/mol (final half-thickness), and then slightly increased to 27.12 kJ/mol (average half-thickness). A similar trend was observed in test II, although lower values decreased from 23.67 kJ/mol to 17.83 kJ/mol and then increased to 21.00 kJ/mol. This variation reflects the influence of shrinkage and geometry on moisture transport [1,15]. The initial half-thickness corresponds to the longest diffusion path, requiring higher energy for moisture migration through intact cellular structures. As drying progresses, shrinkage reduces the diffusion distance and induces structural changes such as cell wall rupture, which facilitate moisture movement and lower the energy barrier. At the final half-thickness, extensive structural collapse and increased porosity further enhance moisture transport, resulting in the lowest activation energy. The average half-thickness provides an intermediate value that more accurately represents the overall diffusion process, accounting for both structural changes and moisture redistribution. Across all characteristic lengths, test I consistently yielded higher activation

energies than test II, with differences ranging from approximately 4.73 to 7.46 kJ/mol. This suggests that moisture migration in test I required more energy, possibly due to a higher initial moisture content, denser tissue structure, minor airflow, temperature uniformity, and sample geometry [53,54]. In contrast, the lower values in test II indicate relatively easier transport, likely due to reduced internal resistance or greater structural softening during drying. The mean E_a ranged from 21.56 to 26.03 kJ/mol across the different characteristic lengths. Variability between tests is reflected in the standard deviation (SD) and coefficient of variation (CV). The initial half-thickness showed the lowest variability (SD = 3.34 kJ/mol; CV = 12.84%), indicating more consistent energy requirements at the early stage of drying when the structure remains intact. The final thickness exhibited the highest variability (SD = 5.28 kJ/mol; CV = 24.47%), likely due to differences in structural deformation and porosity. The average half-thickness showed moderate variability (SD = 4.00 kJ/mol; CV = 16.47%), representing a balanced, stable estimate.

3.7. Estimated Pre-Exponential Factor of the Arrhenius Equation

The pre-exponential factor D_0 is also referred to as the diffusion coefficient constant or Arrhenius factor. The calculated D_0 values with their statistical metrics are presented in Table 5. The values ranged from 8.75×10^{-7} to 1.339×10^{-7} m^2/s, which are consistent with values reported for other agricultural products in the literature [24,28]. The results confirm that the Arrhenius relationship (Equation (8)) adequately describes the temperature dependence of moisture diffusivity in the apple slices. The highest D_0 values were obtained using the initial half-thickness, while the lowest D_0 values corresponded to the final half-thickness, indicating a reduction in diffusion potential as drying progresses. At the initial stage, the tissue structure is relatively open and contains more free water, resulting in greater molecular mobility and higher theoretical diffusivity [41,53]. In contrast, prolonged drying leads to shrinkage and structural collapse, reducing pore connectivity and limiting moisture movement, which is reflected in lower D_0 values. The average half-thickness produces intermediate D_0 values, representing a balance between early-stage free water diffusion and late-stage bound moisture diffusion, and thus better characterizes the overall drying behaviour. The coefficient of variation exceeded 90% for all characteristic lengths, indicating considerable variability between the experimental tests. This is expected as D_0 is derived from the intercept of the Arrhenius plot and is highly sensitive to small variations in diffusivity and temperature. Additionally, the inherent heterogeneity of biological materials, including differences in porosity, composition, and shrinkage behaviour, further contributes to this variability [53,54]. Furthermore, a clear relationship was observed between D_0 (Equation (8)) and E_a (Equation (10)). The initial half-thickness exhibited both high D_0 and E_a, indicating strong temperature-dependence of diffusion. The final half-thickness showed lower D_0 values, reflecting restricted moisture mobility due to structural compaction and reduced water content. The average half-thickness yielded intermediate D_0 and E_a values, representing a balanced condition that realistically describes the overall drying process. D_0 represents the theoretical diffusivity at infinite temperature or the maximum possible diffusivity in the absence of an energy barrier [9,45]. In biological materials such as apple slices, it reflects the intrinsic mobility of water molecules within the matrix, that is, how easily they could move if not limited by structural resistance or bonding energy. Higher D_0 values indicate more open pathways and greater inherent mobility, while lower values suggest restricted diffusion due to dense tissue structure, strong intermolecular bonding or limited pore connectivity [38,42].

Table 5. Determined pre-exponential factor across characteristic lengths for duplicated tests.

Tests	Characteristic Length, L (m)	Pre-Exponential Factor D_0 (m^2/s)
I	Initial	1.740×10^{-5}
II		3.012×10^{-6}
I	Final	2.193×10^{-6}
II		1.339×10^{-7}
I	Average	7.231×10^{-6}
II		8.750×10^{-7}

3.8. Comparison of Experimental and Theoretical Effective Moisture Diffusivity

Using (Equation (11)), the theoretical effective moisture diffusivity, $D_{eff\,th}$ was computed and compared with the experimentally determined D_{eff} values. The results are presented in Table 6 and illustrated in Figure 6 for different characteristic lengths and drying temperatures.

$$D_{eff\,th} = D_0 \exp - \frac{E_a}{RT} \quad (11)$$

Table 6. Experimental and predicted effective moisture diffusivity across characteristic lengths and drying temperature of dried apple slices for duplicated tests.

Tests	Characteristic Length, L (m)	T_{PR} (°C)	D_{eff} (Experimental) $\times 10^{-10}$ (m^2/s)	$D_{eff\,th}$ (Predicted) $\times 10^{-10}$ (m^2/s)
I	Initial	40	3.077	3.187
I		50	4.170	4.467
I		60	7.458	6.135
I		70	8.026	8.271
I		80	10.309	10.964
I	Final	40	1.631	1.325
I		50	1.433	1.790
I		60	2.251	2.375
I		70	2.833	3.099
I		80	4.666	3.983
I	Average	40	2.297	2.165
I		50	2.623	2.988
I		60	4.476	4.045
I		70	5.099	5.381
I		80	7.212	7.043
II	Initial	40	3.739	3.393
II		50	4.125	4.495
II		60	5.406	5.856
II		70	7.605	7.511
II		80	10.050	9.501
II	Final	40	1.580	1.422
II		50	1.623	1.758
II		60	2.041	2.145
II		70	2.324	2.587
II		80	3.520	3.088
II	Average	40	2.545	2.301
II		50	2.731	2.970
II		60	3.523	3.775
II		70	4.585	4.731
II		80	6.367	5.854

D_{eff}: Effective moisture diffusivity.

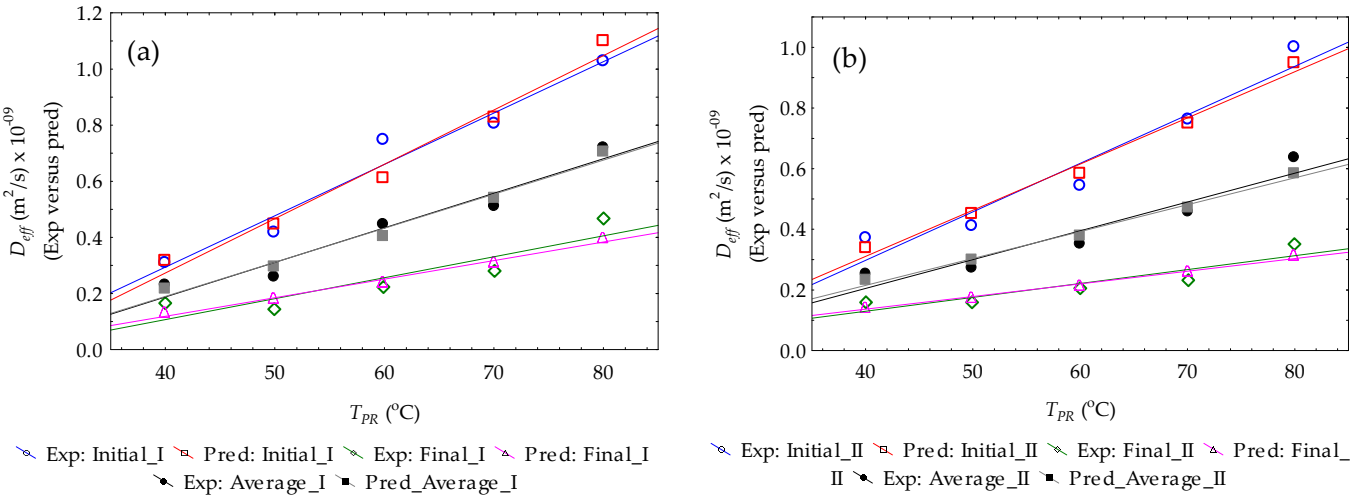

Figure 6. Experimental and predicted effective moisture diffusivity (D_{eff}) against drying temperature across characteristic lengths for duplicated tests (**a**) test I and (**b**) test II.

For all characteristic lengths under both tests, effective moisture diffusivity increased linearly with temperature, consistent with the expected Arrhenius-type behaviour. Higher drying temperature accelerates internal moisture migration by increasing molecular mobility and vapour pressure gradients. Both experimental and predicted values followed this linear trend, confirming that the Arrhenius model adequately describes the temperature dependence of diffusion [35,36]. The two experimental tests showed similar diffusivity patterns, indicating good repeatability of the measurements. The average characteristic length provided the most representative estimates of D_{eff}, as it accounts for both the initial geometry and the effects of shrinkage during drying.

The statistical performance indicators obtained from the comparison between the experimental and predicted effective moisture diffusivity are presented in Table 7. The high coefficient of determination (R^2) values ranging from 0.886 to 0.965, consistent with the model efficiency (EF) values, and the low values of the root mean square error (RMSE), mean absolute error (MAE) and mean absolute percentage error (MAPE) confirm that the Arrhenius model suitably fits the experimental diffusivity data across the temperature range studied. The percentage error (% error) ranged from 0.29 to1.38%, indicating high model accuracy. However, the negative bias values (−0.29 to −1.38%) prior to absolute transformation suggest a slight tendency of the model to underpredict diffusivity, particularly at the final characteristic length. Among the three characteristic lengths, the average length yielded the highest R^2 value of 0.965, indicating that it provides the most realistic representation of the actual diffusion path length during drying. This result suggests that the average dimension effectively accounts for both the initial tissue geometry and shrinkage effects, resulting in more accurate diffusivity estimation. The initial length (R^2) value of 0.951 also showed strong agreement, representing diffusion behaviour before significant structural deformation. In contrast, the final length exhibited a slightly lower (R^2) value of 0.886 and the highest MAPE (12%), likely due to the increased structural collapse, internal resistance, and porosity changes occurring in the later stages of drying.

Table 7. Statistical metrics for evaluating the experimental and predicted effective moisture diffusivity of dried apple slices during convective drying.

Characteristic Lengths, L (m)	R^2	RMSE	MAE	MAPE	EF	% Error
Initial	0.951	5.580×10^{-11}	4.440×10^{-11}	7.105	0.951	0.293
Average	0.965	3.010×10^{-11}	2.770×10^{-11}	7.393	0.965	0.487
Final	0.886	3.290×10^{-11}	2.830×10^{-11}	12.021	0.886	1.385

R^2: Coefficient of determination, RMSE: Root mean square error, MAE: Mean absolute error, MAPE: Mean absolute percentage error and EF: Model efficiency.

4. Limitations

The calculated drying parameters were generally interpreted as apparent drying characteristics because the simplified approach assumed negligible moisture content and temperature-dependent dry-mass basis. Future studies should compare these with those obtained using a reference method based on true dry mass and equilibrium moisture content of the apple slices to further evaluate the accuracy, applicability and limitations of the simplified drying method. In addition, rigorous statistical validation of the drying models and parameter estimation based on several experimental trials should be emphasized. Energy consumption, texture, nutritional and sensory qualities should also be evaluated.

5. Conclusions

The moisture content versus time curves described the overall drying behaviour of apple slices and demonstrated the influence of drying temperatures on moisture removal kinetics. Higher temperatures exhibited the fastest reduction in moisture content, while lower temperatures showed the slowest drying behaviour. The elevated moisture content curves observed at higher temperatures occurred because of the simplified approach calculation, which assumed the final drying mass to represent the true dry mass of the material. The moisture ratio curves across the drying temperatures began at unity since it is a normalized parameter, and this normalization process minimizes scaling differences. A polynomial trend was observed to fit the shrinkage and temperature behaviour of dried apple slices with a high coefficient of determination (R^2) of 0.985 in comparison with a linear trend, which produced (R^2) of 0.249. The calculated effective moisture diffusivity (D_{eff}) values ranged from 1.43×10^{-10} to 10.31×10^{-10} m^2/s, which increased with drying temperature. The average half-thickness provided a more realistic estimate of D_{eff}, representing the mean diffusion distance throughout the drying process. The initial half-thickness tends to overestimate D_{eff}, as it assumes a constant diffusion path despite the occurrence of shrinkage, whereas the final half-thickness underestimates D_{eff} because it represents only the end-stage geometry when diffusion is minimal. Across the half-thickness characteristic lengths, the activation energy (E_a) values ranged from 21.56 ± 5.28 to 26.03 ± 4.00 kJ/mol, where the final half-thickness produced the lowest E_a, which assumes the smallest diffusion path throughout the drying process. However, the average half-thickness of 24.29 ± 4.00 kJ/mol represents an intermediate estimate of the temperature sensitivity of moisture diffusion, as it accounts for the reduction in diffusion path length caused by shrinkage during drying. The pre-exponential factor D_0 values ranged from 8.75×10^{-7} to 1.339×10^{-7} m^2/s. The low values of the root mean square error (RMSE) and mean absolute error (MAE), together with high model efficiency (EF), demonstrated a strong agreement between the experimental and predicted D_{eff} values, thereby confirming the suitability of the Arrhenius model for describing the temperature dependence of moisture diffusion. These findings suggest that the simplified approach

adopted in this study provides physically reasonable drying parameters. Nevertheless, further validation is required using a reference method as indicated in the study limitations.

Author Contributions: Conceptualization. O.D., A.K., Č.M. and D.H.; Methodology. O.D., A.K., Č.M. and A.S.; Validation. O.D., A.K., Č.M., A.S. and D.H.; Formal analysis. O.D., A.K., Č.M., A.S. and D.H.; Data curation. O.D., A.K., Č.M. and A.S.; Writing—original draft. O.D., A.K. and Č.M.; Writing—review and editing. O.D., A.K., Č.M. and D.H. All authors have read and agreed to the published version of the manuscript.

Funding: The study was supported by the Internal Grant Agency of the Czech University of Life Sciences Prague, Grant Number: IGA Project Number—2024:31130/1312/3108.

Data Availability Statement: The original contributions presented in this study are included in the article. Further inquiries can be directed to the corresponding author.

Conflicts of Interest: The authors declare no conflicts of interest.

References

1. Bai, J.-W.; Zhang, L.; Aheto, J.H.; Cai, J.-R.; Sun, L.; Tian, X.-Y. Effects of different pretreatment methods on drying kinetics, three-dimensional deformation, quality characteristics and microstructure of dried apple slices. *Innov. Food Sci. Emerg. Technol.* **2023**, *83*, 103216. [CrossRef]
2. Joardder, M.U.H.; Karim, M.A. Drying kinetics and properties evolution of apple slices under convective and intermittent-MW drying. *Therm. Sci. Eng. Prog.* **2022**, *30*, 101279. [CrossRef]
3. Joardder, M.U.H.; Karim, A.; Kumar, C. Effect of temperature distribution on predicting quality of microwave dehydrated food. *J. Mech. Eng. Sci.* **2013**, *5*, 562–568. [CrossRef]
4. Orsat, V.; Yang, W.; Changrue, V.; Raghavan, G.S.V. Microwave-assisted drying of biomaterials. *Food Bioprod. Process.* **2007**, *85*, 255–263. [CrossRef]
5. Amanor-Atiemoh, R.; Zhou, C.; Wahia, H.; Mustapha, A.T.; Zhou, R. Acoustically-aided osmo-dehydration pretreatments under pulsed vacuum dryer for apple slices: Drying kinetics, thermodynamics, and quality attributes. *J. Food Sci.* **2020**, *85*, 3909–3919. [CrossRef] [PubMed]
6. Kaleta, A.; Gornicki, K.; Winiczenko, R.; Chojnacka, A. Evaluation of drying models of apple (var. Ligol) dried in a fluidized bed dryer. *Energy Convers. Manag.* **2013**, *67*, 179–185. [CrossRef]
7. Baysal, T.; Ozbalta, N.; Gokbulut, S.; Capar, B.; Gurlek, G. Investigation of effects of various drying methods on the quality characteristics of apple slices and energy efficiency. *Therm. Sci. Technol.* **2015**, *35*, 135–144.
8. Alibas, I. Microwave, air and combined microwave–air-drying parameters of pumpkin slices. *LWT–Food Sci. Technol.* **2007**, *40*, 1445–1451. [CrossRef]
9. Kidane, H.; Farkas, I.; Buzas, J. Performance evaluation of solar drying chambers and drying kinetics of apple slices. *Energy Rep.* **2025**, *13*, 4528–4540. [CrossRef]
10. Kidane, H.; Farkas, I.; Buzas, J. Mathematical modelling of golden apple drying and performance evaluation of solar drying systems using energy and exergy approach. *Sci. Rep.* **2025**, *15*, 7805. [CrossRef] [PubMed]
11. Chen, C.; Venkitasamy, C.; Zhang, W.; Khir, R.; Upadhyaya, S.; Pan, Z. Effective moisture diffusivity and drying simulation of walnuts under hot air. *Int. J. Heat Mass Transf.* **2020**, *150*, 119283. [CrossRef]
12. Rabha, D.K.; Muthukumar, P. Performance studies on a forced convection solar dryer integrated with a paraffin wax-based latent heat storage system. *Sol. Energy.* **2017**, *149*, 214–226. [CrossRef]
13. Mujumdar, A.S. Research and development in drying: Recent trends and future prospects. *Dry. Technol.* **2004**, *22*, 1–26. [CrossRef]
14. Zhang, W.; Pan, Z.; Xiao, H.; Zheng, Z.; Chen, C.; Gao, Z. Pulsed vacuum drying (PVD) technology improves drying efficiency and quality of Poria cubes. *Dry. Technol.* **2018**, *36*, 908–921.
15. Mayor, L.; Sereno, A.M. Modelling shrinkage during convective drying of food materials: A review. *J. Food Eng.* **2004**, *61*, 373–386. [CrossRef]
16. Karathanos, V.T.; Villalobos, G.; Saravacos, G.D. Comparison of two methods of estimation of the effective moisture diffusivity from drying data. *J. Foods Sci.* **1990**, *55*, 218–231. [CrossRef]
17. Ning, Z.; Khir, R.; Niederholzer, F.; Pan, Z. Characteristics of moisture diffusivity and shrinkage evolution of in-hull almonds under hot air drying. *LWT–Food Sci. Technol.* **2025**, *232*, 118455. [CrossRef]
18. Rafiee, S.; Sharifi, M.; Keyhani, A.; Omid, M.; Jafari, A.; Mohtasebi, S.S.; Mobli, H. Modeling effective moisture diffusivity of orange slice (Thompson CV.). *Int. J. Food Prop.* **2010**, *13*, 32–40. [CrossRef]

19. Kayran, S.; Doymaz, I. Infrared drying and effective moisture diffusivity of apricot halves: Influence of pretreatment and infrared power. *J. Food Process. Preserv.* **2017**, *41*, e12827.
20. Crank, J. *The Mathematics of Diffusion*; Oxford University Press, Inc.: Oxford, UK, 1975.
21. Akhijani, H.S.; Abrahosseini, A.; Kianmehr, M.H. Effective moisture diffusivity during hot air solar drying of tomato slices. *Res. Agric. Eng.* **2016**, *62*, 15–23. [CrossRef]
22. Babalis, S.J.; Belessiontis, V.G. Influence of the drying conditions on the drying constants and moisture diffusivity during the thin-layer drying of figs. *J. Food Eng.* **2004**, *65*, 449–458. [CrossRef]
23. Kumar, R.; Sharma, A.K.; Agnihotri, K. Dynamics of an innovation diffusion model with time delay. *East Asian J. Appl. Math.* **2017**, *7*, 455–481. [CrossRef]
24. Barforoosh, M.Y.; Borghaee, A.M.; Rafiee, S.; Minaei, S.M.; Beheshti, B. Determining the effective diffusivity coefficient and activation energy in thin-layer drying of Haj Kazemi peach slices and modeling drying kinetics using ANFIS. *Int. J. Low-Carbon Technol.* **2024**, *19*, 192–206. [CrossRef]
25. Younas, S.; Arqam, U.; Wang, X.; Liu, C.; Huang, Y.; Feng, L. Ultrasound-assisted controlled ice-seeding during freezing: Impact on quality attributes, freeze drying kinetics, structural modification, supercooling suppression and moisture mobility of apple. *Food Control* **2026**, *181*, 111761. [CrossRef]
26. Subrahmanyam, K.; Gul, K.; Paridala, S.; Sehrawat, R.; More, K.S.; Dwivedi, M.; Jaddu, G. Effect of cold plasma pretreatment on drying kinetics and quality attributes of apple slices in refractance window drying. *Innov. Food Sci. Emerg. Technol.* **2024**, *92*, 103594. [CrossRef]
27. Dajbych, O.; Kabutey, A.; Mizera, Č.; Herák, D. Investigation of the effects of infrared and hot air oven drying methods on drying behaviour and colour parameters of red delicious apple slices. *Process* **2023**, *11*, 3027. [CrossRef]
28. Pinheiro, M.N.C.; Castro, L.M.M.N. Effective moisture diffusivity prediction in two Portuguese fruit cultivars (Bravo de Esmolfe apple and Madeira banana) using drying kinetics data. *Heliyon* **2023**, *9*, e17741. [CrossRef] [PubMed]
29. Pinheiro, M.N.C.; Madaleno, R.O.; Castro, L.M.M.N. Drying kinetics of two fruits Portugues cultivars (Bravo de Esmolfe apple and Madeira banana): An experimental study. *Heliyon* **2022**, *8*, e09341. [CrossRef] [PubMed]
30. Chen, A.; Achkar, G.E.L.; Liu, B.; Bennacer, R. Experimental study on moisture kinetics and microstructure evolution in apples during high power microwave drying process. *J. Food Eng.* **2021**, *292*, 110362. [CrossRef]
31. Bi, J.; Yang, A.; Liu, X.; Wu, X.; Chen, X.; Wang, Q.; Lv, J.; Wang, X. Effects of pretreatments on explosion puffing drying kinetics of apple chips. *LWT–Food Sci. Technol.* **2015**, *60*, 1136–1142. [CrossRef]
32. Mujumdar, A.S. *Handbook of Industrial Drying*, 3rd ed.; Taylor & Francis Group CRC: Boca Raton, FL, USA, 2006.
33. Khater, E.-S.G.; Bahnasawy, A.H.; Elwakeel, A.E.; Tantawy, A.A.; Elbeltagi, A.; Salem, A.; Marey, S.A.; Okasha, A.M.; Metwally, K.A. Comparative analysis of drying kinetics, thermodynamic properties, and mathematical modeling of pomegranate peel (*Punica granatum* L.) in a hybrid solar dryer and an oven dryer. *Sci. Rep.* **2025**, *15*, 26288. [CrossRef] [PubMed]
34. Wang, H.; Liu, Z.-L.; Vidyarthi, S.K.; Wang, Q.-H.; Gao, L.; Li, B.-R.; Wei, Q.; Liu, Y.-H.; Xiao, H.-W. Effects of different drying methods on drying kinetics, physicochemical properties, microstructure, and energy consumption of potato (*Solanum tuberosum* L.) cubes. *Dry. Technol.* **2021**, *39*, 418–431.
35. Xie, Y.; Lin, Y.; Li, X.; Yang, H.; Han, J.; Shang, C.; Li, A.; Xiao, H.; Lu, F. Peanut drying: Effects of various drying methods on drying kinetic models, physicochemical properties, germination characteristics, and microstructure. *Inf. Process. Agric.* **2022**, *10*, 447–458.
36. Komolafe, C.A.; Ojediran, J.O.; Ajao, F.O.; Dada, O.A.; Afolabi, Y.T.; Oluwaleye, I.O.; Alake, A.S. Modelling of moisture diffusivity during solar drying of locust beans with thermal storage material under forced and natural convection mode. *Case Stud. Therm. Eng.* **2019**, *15*, 100542. [CrossRef]
37. Dina, S.F.; Ambarita, H.; Napitupulu, F.H.; Kawai, H. Study on effectiveness of continuous solar dryer integrated with desiccant thermal storage for drying cocoa beans. *Case Stud. Therm. Eng.* **2015**, *5*, 32–40. [CrossRef]
38. Xiao, H.W.; Pang, C.L.; Wang, L.H.; Bai, J.W.; Yang, W.X.; Gao, Z.J. Drying kinetics and quality of Monukka Seedless grapes dried in an air–impingement jet dryer. *Biosyst. Eng.* **2010**, *105*, 233–240. [CrossRef]
39. Zhang, J.; Karim, A.; Sutar, P.P.; Mujumdar, A.S.; Wang, Z.-X.; Shi, Y.-S.; Liu, S.-L.; Lv, W.-Q.; Xiao, H.-W. Sustainable development of drying technologies for agricultural products: Recent advances, challenges, and future prospects. *Renew. Sustain. Energy Rev.* **2026**, *226*, 116419. [CrossRef]
40. Li, C.; Ren, G.; Zhang, L.; Duan, X.; Wang, Z.; Ren, X.; Chu, Q.; He, T. Effects of different drying methods on the drying characteristics and drying quality of *Cistanche deserticola*. *LWT-Food Sci. Technol.* **2023**, *184*, 115000. [CrossRef]
41. Mugi, V.R.; Chandramohan, V. Shrinkage, effective diffusion coefficient, surface transfer coefficients and their factors during solar drying of food products—A review. *Sol. Energy* **2021**, *229*, 84–101. [CrossRef]
42. Gilago, M.C.; Mugi, V.R.; Chandramohan, V.P. Evaluation of drying kinetics of carrot and thermal characteristics of natural and forced convection indirect solar dryer. *Results Eng.* **2023**, *18*, 101196. [CrossRef]
43. Statsoft Inc. *STATISTICA for Windows*; Statsoft Inc.: Tulsa, OK, USA, 2013.

44. Yilmaz, M.S.; Sakiyan, O.; Isci, A. Effect of different pretreatments on drying characteristics and physicochemical properties of apricot (*Prunus armeniaca* L.). *J. Food Process Eng.* **2024**, *47*, e14757. [CrossRef]
45. Arulkumar, M.; Pandian, N.K.S.; Murugan, B.; Nambi, V.E.; Sivaranjani, S.; Baskaran, D.; Pugazhenthi, T.R.; Kishore, S.G.; Pandiselvam, R. Drying kinetics, effective moisture diffusivity and activation energy of osmotic pretreated hot-air-dried paneer cubes. *J. Food Process. Preserv.* **2023**, *2023*, 7685192. [CrossRef]
46. Akpinar, E.K. Mathematical modelling of thin layer drying process under open sun of some aromatic plants. *J. Food Eng.* **2006**, *77*, 864–870. [CrossRef]
47. Doymaz, I. Convective air-drying characteristics of thin layer carrots. *J. Food Eng.* **2004**, *61*, 359–364. [CrossRef]
48. Madamba, P.S.; Driscoll, R.H.; Buckle, K.A. The thin-layer drying characteristics of garlic slices. *J. Food Eng.* **1996**, *29*, 75–97. [CrossRef]
49. Diamante, L.M.; Munro, P.A. Mathematical modelling of thin layer solar drying of sweet potato slices. *Sol. Energy* **1993**, *51*, 271–276. [CrossRef]
50. Ramakrishnan, S.R.; Chelliah, R.; Antony, U.; Oh, D.-H. Characterization of drying kinetics and moisture diffusivity in finger millet using fluidized bed drying. *J. Stored Prod. Res.* **2025**, *113*, 102700. [CrossRef]
51. Cavalcanti-Mata, M.E.; Duarte, M.E.; Tolentino, M.; Mendes, F.A.; Batista, L.; de Lima, J.M.; Lucio, A.; Nascimento, A.P.; Almeida, R.D.; Lisboa, H.M. Drying kinetics of industrial pineapple waste: Effective diffusivity and thermodynamics properties resulting from new mathematical models derived from the Fick equation. *Processes* **2024**, *12*, 1198. [CrossRef]
52. Zogzas, N.; Maroulis, Z.; Marinos-Kouris, D. Moisture diffusivity data compilation in foodstuffs. *Dry. Technol.* **1996**, *14*, 2225–2253. [CrossRef]
53. Koua, B.K.; Koffi, P.M.E.; Gbaha, P. Evolution of shrinkage, real density, porosity, heat and mass transfer coefficients during indirect solar drying of cocoa beans. *J. Saudi Soc. Agric. Sci.* **2019**, *18*, 72–82. [CrossRef]
54. Li, L.; Zhang, M.; Zhou, L. A promising pulse-spouted microwave freeze drying method used for Chinese yam cubes dehydration: Quality, energy consumption, and uniformity. *Dry. Technol.* **2019**, *39*, 148–161. [CrossRef]
55. Hatamipour, M.S.; Mowla, D. Shrinkage of carrots during drying in an inert medium fluidized bed. *J. Food Process Eng.* **2002**, *55*, 247–252. [CrossRef]
56. Waheed, M.A.; Komolafe, C.A. Temperatures dependent drying kinetics of cocoa beans varieties in air-ventilated oven. *Front. Heat Mass Transf.* **2018**, *12*, 1–7. [CrossRef]
57. Tulek, Y. Drying kinetics of oyster mushroom (*Pleurotus ostreatus*) in a convective hot air dryer. *J. Agric. Sci. Technol.* **2011**, *13*, 655–664.
58. Mirzaee, E.; Rafiee, S.; Keyhani, A.; Emam-Djomeh, Z. Determining of moisture diffusivity and activation energy in drying of apricots. *Res. Agric. Eng.* **2009**, *55*, 114–120. [CrossRef]
59. Komolafe, C.A.; Oluwaleye, I.O.; Adejumo, A.O.D.; Waheed, M.A.; Kuye, S.I. Determination of moisture diffusivity and activation energy in the convective drying of fish. *Int. J. Heat Technol.* **2018**, *36*, 1262–1267. [CrossRef]

Disclaimer/Publisher's Note: The statements, opinions and data contained in all publications are solely those of the individual author(s) and contributor(s) and not of MDPI and/or the editor(s). MDPI and/or the editor(s) disclaim responsibility for any injury to people or property resulting from any ideas, methods, instructions or products referred to in the content.